PROTEINS: Structure, Function, and Genetics 12:75–86 (1992)

Subunit Assembly and Active Site Location in the Structure of Glutamate Dehydrogenase

Patrick J. Baker, K. Linda Britton, Paul C. Engel, George W. Farrants, Kathryn S. Lilley, David W. Rice, and Timothy J. Stillman

Department of Molecular Biology and Biotechnology, Krebs Institute for Biomolecular Research, University of Sheffield, Sheffield S10 2TN, United Kingdom

ABSTRACT **The three-dimensional crystal structure of the NAD^+-linked glutamate dehydrogenase from *Clostridium symbiosum* has been solved to 1.96 Å resolution by a combination of isomorphous replacement and molecular averaging and refined to a conventional crystallographic *R* factor of 0.227. Each subunit in this multimeric enzyme is organised into two domains separated by a deep cleft. One domain directs the self-assembly of the molecule into a hexameric oligomer with 32 symmetry. The other domain is structurally similar to the classical dinucleotide binding fold but with the direction of one of the strands reversed. Difference Fourier analysis on the binary complex of the enzyme with NAD^+ shows that the dinucleotide is bound in an extended conformation with the nicotinamide moiety deep in the cleft between the two domains. Hydrogen bonds between the carboxyamide group of the nicotinamide ring and the side chains of T209 and N240, residues conserved in all hexameric GDH sequences, provide a positive selection for the *syn* conformer of this ring. This results in a molecular arrangement in which the A face of the nicotinamide ring is buried against the enzyme surface and the B face is exposed, adjacent to a striking cluster of conserved residues including K89, K113, and K125. Modeling studies, correlated with chemical modification data, have implicated this region as the glutamate/2-oxoglutarate binding site and provide an explanation at the molecular level for the B type stereospecificity of the hydride transfer of GDH during the catalytic cycle.**

Key words: crystallography, protein structure, refinement, dinucleotide binding domain

INTRODUCTION

Glutamate dehydrogenases (GDH) (EC 1.4.1.2–4), as a class, catalyze the reversible oxidative deamination of L-glutamate to 2-oxoglutarate and ammonia using NAD^+ or $NADP^+$ as a cofactor[1]:

$$\text{Glutamate} + \text{NAD(P)}^+ + H_2O \rightleftharpoons \text{2-Oxoglutarate} + NH_4^+ + \text{NAD(P)H}.$$

This reaction permits the interconversion of free ammonium ions and α-amino nitrogen and, in conjunction with aminotransferases, GDH serves as a clearing house for α-amino groups.[2] In general within biological systems, processes of oxidative degradation are NAD^+ linked, while the specificity of enzymes for $NADP^+$ is restricted with few exceptions to reactions of reductive biosynthesis. Thus within the GDH family, the members involved in glutamate catabolism are NAD^+-dependent, whereas those involved in ammonia assimilation are $NADP^+$-linked. The dual coenzyme specificity found in higher organisms, with very similar affinities for NAD^+ and $NADP^+$, may reflect an amphibolic role.

GDHs have been isolated and sequenced from a number of varied sources and fall into two oligomeric classes. The bacterial and fungal $NADP^+$-linked and vertebrate dual-specificity GDHs have six identical subunits, with a subunit M_r between 48,000 (bacterial) and 55,000 (vertebrate),[3] whereas the NAD^+-linked enzymes have either four identical subunits with an M_r of approximately 115,000 (e.g., *Saccharomyces cerevisiae*,[4] *Neurospora crassa*[5]) or six identical subunits with a subunit M_r of approximately 48,000 (*Peptostreptococcus asaccharolyticus*,[6] *Clostridium symbiosum*[7]). Sequence comparisons for GDHs from *Escherichia coli*,[8] *P. asaccharolyticus* (B. Snedecor, personal communication), *N. crassa*,[9] *Salmonella typhimurium*,[10] bovine liver,[11] chicken liver,[11] human liver,[12] and rat liver[3] show that the hexameric enzymes are structurally homologous whatever their coenzyme specificity. Specifically, the homology is poor for the N-terminal 50 residues and then becomes strong for the next 350 residues. At the C-terminus the homology can

Received August 6, 1990; revision accepted June 10, 1991.

Address reprint requests to Dr. David W. Rice, The Department of Molecular Biology and Biotechnology, The University of Sheffield, P.O. Box 594, Firth Court, Western Bank, Sheffield S10 2UH, United Kingdom.

Present addresses: George W. Farrants: Norwegian Radium Hospital, Montebello, N-0310, Oslo 3, Norway. Kathryn S. Lilley: Department of Biochemistry, Adrian Building, University of Leicester, Leicester LE1 7RH, United Kingdom.

be divided into two classes, nonvertebrate and vertebrate. The nonvertebrate enzymes are all closely related, while the vertebrate GDHs show little homology to the other class in this region and, furthermore, contain an additional 50 residues.[13] Chemical modification studies have implicated the C-terminal region of the bovine enzyme in the allosteric response to GTP.[14–16] The relationship between the hexameric and tetrameric enzymes is less clear, but the existence of a low level of sequence homology between the C-terminal portion of the NAD^+-linked tetrameric enzyme from *N. crassa* and a consensus sequence from the hexameric enzymes probably implies a remote evolutionary relationship and a related polypeptide fold.[17]

The hexameric glutamate dehydrogenases have been the subject of many biochemical studies which have investigated properties such as reversible polymerization at high protein concentration,[18–20] activation–inactivation phenomena which are both pH dependent and also affected by the presence of small ligands,[21–23] and allosteric regulation.[24–27] Chemical modification studies[28] and, more recently, site-directed mutagenesis[29] have been used to highlight the functional roles played by key residues in the sequence and, in particular, have implicated lysyl residues in catalytic activity. However, for a complete understanding of the effects of these changes, the three-dimensional framework provided by a crystallographic structure determination is essential.

Here we report the determination of the atomic structure of the hexameric NAD^+-linked GDH from *C. symbiosum* to 1.96 Å resolution by X-ray diffraction. The location of the dinucleotide binding site by difference Fourier analysis and patterns of sequence homology lead to a proposed active site model and an explanation of the molecular basis for the stereospecificity of the hydride transfer.

MATERIALS AND METHODS

Data Collection

GDH was isolated and purified from centrifuged sonic extracts of *C. symbiosum* using a single step procedure with a Remazol-red dye-linked Sepharose 4B affinity column.[7] Crystals of this enzyme, grown using the method of vapor diffusion from 35% saturated $(NH_4)_2SO_4$ at pH 7.0, belong to the monoclinic space group $C2$ with cell dimensions a = 147.1 Å, b = 151.3 Å, c = 94.6 Å, and β = 132.75° with a trimer in the asymmetric unit.[30] Diffractometer data were collected on the native crystals to 3.7 Å in discrete overlapping resolution shells on the modified Hilger and Watts multicounter 5 circle diffractometer in the Laboratory of Molecular Biophysics, University of Oxford, with Ni-filtered CuK_α radiation. These data were corrected for absorption using the empirical method of North et al.[31] Two further native data sets were collected on a rotation camera using the S.E.R.C. Synchrotron Radiation Source (SRS) at Daresbury. One data set, to 2.5 Å resolution, was collected from 5 different crystals predominantly on station 7.2 with a wavelength of 1.488 Å, and the other to 1.96 Å resolution, using a total of eight crystals, on station 9.6 with a wavelength of 0.88 Å. The 3.7 and 2.5 Å data sets were scaled and merged together using the method of Fox and Holmes[32] to produce a single data set to 2.5 Å. Analysis of the 2.5 and 1.96 Å data sets showed that the 1.96 Å data set was of a significantly higher quality in the 2.5 Å resolution shell. A major contributory factor to this difference in quality is likely to be the reduction in absorption at the shorter wavelength used for the data collection, which is particularly marked for these anisotropically shaped GDH crystals. The 2.5 Å data were scaled to the 1.96 Å data set and data missing from the latter (principally overloaded reflections at low resolution) were filled in from the 2.5 Å set. Data on two related mercury derivatives [2,5-bis(bromomercurimethyl)tetrahydrofuran (DBMMF) and ethyl mercury phosphate (EMP)] were collected to 2.5 Å on the SRS, again using the rotation camera method. Data were collected for the DBMMF derivative from two crystals on station 7.2 at a wavelength of 1.488 Å and for the EMP derivative from three crystals on station 9.6 at a wavelength of 0.86 Å. This incident beam energy is just on the high energy side of the L_{II} mercury absorption edge and was chosen to maximize the anomalous scattering signal from the mercury atom.[33] Each derivative data set was merged and scaled to the native data separately. In addition, a 2.5 Å data set was collected on station 7.2 at the SRS with a wavelength of 1.488 Å on a crystal which had been soaked in a 5 mM solution of the coenzyme NAD^+. Unless otherwise stated all data were processed and analyzed using the CCP4 suite of programs.[34]

Phase Determination

Initial positions of the mercury-binding sites were obtained from a difference Fourier at 6 Å, using the phases from the 6 Å structure determination.[30] Both derivatives showed a similar substitution pattern, with two mercury-binding sites per subunit, one of which was fully occupied in all three subunits while the other had different occupancies. The mercury peak shape in the DBMMF derivative was distinctly elongated in one direction and the size and shape of this extra feature were fully consistent with its assignment to a bromine atom. On the high occupancy sites where these features were significant the sites were modeled in the refinement as two atoms. The derivatives were refined using the F_{HLE} method of Dodson and Vijayan[35] and an MIR map was calculated to 2.5 Å resolution. The noncrystallographic 3-fold axis was initially determined using the mean of the 3-fold related heavy atom positions and the 32

TABLE I. Structure Determination Statistics*

a. Data collection and isomorphous replacement

Data set	Resolution (Å)	Number of crystals	Reflections Measured	Reflections Unique	Complete data (%)	R_{merge} (all data)	Mean fractional isomorphous difference	rms F_{HCALC}/E	R_K	R_{PR}
Native	1.96	7	336,059	101,125	93	0.073	—	—	—	—
Native	2.5	5	202,299	40,258	83	0.105	—	—	—	—
Native	3.7	1	15,898	14,898	92	0.079	—	—	—	—
EMP	2.5	3	174,050	40,461	83	0.092	0.186	1.94	0.127	0.078
DBMMF	2.5	2	100,787	34,845	72	0.140	0.267	1.79	0.204	0.138

b. Molecular averaging

Map identifier	Number of cycles	FOM	Correlation coefficient	R_{AV}
AVMAP1	18	0.78	0.840	0.310
AVMAP2	10	0.78	0.864	0.275

*For the real space averaging, the initial isomorphous map was averaged for 18 cycles increasing the resolution stepwise to 2.5 Å, the final electron density map was called AVMAP1. All derivatives were then rerefined using the combined phases from AVMAP1. A new isomorphous map was calculated and averaged for 10 cycles at 2.5 Å to give AVMAP2. R_{merge} is $\Sigma_{hkl}|I_1-I_m|/\Sigma_{hkl}I_m$, where I_i and I_m are the observed intensity and mean intensity of related reflections, respectively. F_{HCALC} is the heavy atom structure factor, E is the residual lack of closure. R_K is the "Kraut" R factor = $\Sigma|(|F_{PHOBS}|-|F_P|)| / \Sigma|F_{PHOBS}|$. R_{PR} is the phase refined R = $\Sigma|(|F_{PHOBS}|-|F_{PHCALC}|)| / \Sigma|F_{PHOBS}|$. FOM is the overall figure of merit, the correlation coefficient = $\Sigma(\langle F_h\rangle-|F_o|)\,(\langle F_h\rangle-|F_c|)/[\Sigma(\langle F_h\rangle-|F_o|)^2\,(\langle F_h\rangle-|F_c|)^2]^{1/2}$, where $|F_o|$ and $|F_c|$ are the observed and calculated structure factor amplitudes placed on the same relative scale for each resolution shell and $\langle F_h\rangle$ is the mean observed amplitude in that shell. $R_{AV}=\Sigma|(|F_o|-|F_{CAV}|)| / \Sigma|F_o|$, where $|F_{CAV}|$ are the structure factor amplitudes calculated from the averaged map.

symmetry point at the center of the hexamer. A molecular boundary for the trimer was constructed by visual inspection of the MIR map and this map was averaged, within the boundary, about the noncrystallographic 3-fold axis, using the real space algorithm of Bricogne.[36] Both derivatives were then refined again by the method of "phase refinement"[37] using the combined isomorphous and averaged phases but selecting only those reflections with an overall figure of merit greater than 0.9. A new MIR map, with a figure of merit for the phases to 2.5 Å of 0.57, was calculated and then reaveraged about the 3-fold axis for 10 cycles at a resolution of 2.5 Å. Full statistics on the data collection, phasing, and averaging are shown in Table I. Visual inspection of this electron density map enabled a tentative tracing of the polypeptide chain to be made and an atomic model was constructed using the program FRODO[38] running on an Evans and Sutherland PS300 attached to a microVAX II. Initially, as no sequence was available, the side chains in this model were built as either alanine or glycine. Subsequently, the assignment of side chains was based on a partial amino acid sequence on this GDH, which became available in parallel with the refinement of the structure, and which was derived from automated sequencing of both the intact protein and a number of peptides produced by tryptic or CNBr digestion.[58] The initial sequence fitting to the model comprised placing a peptide derived from N-terminal sequencing (1–51) and two cysteine containing peptides (142–147 and 312–326) to the electron density map. The close proximity of the mercury-binding sites to the cysteine positions gave confidence in the general correctness of the connectivity. The sequenced peptides now account for some 75% of the structure and, given the close homology to the $NADP^+$-dependent GDH from *E. coli* (52% identities over 332 residues compared), the peptide fragments can be confidently placed within the overall sequence.

Refinement

During the course of model building, sequence fitting, and refinement only those side chains which could be unambiguously fitted to the electron density were assigned, while for others, where the electron density was less clear, a truncated side chain was used. As more peptide sequence became available it was included where appropriate. Side chain residues in the current model falling outside the sequenced peptides, which are suffixed X in this paper, were surmised from the shape of the electron density coupled with an inspection of the aligned sequences of the hexameric GDHs. The model was improved by iterative refinement using the TNT package.[39] For each round of refinement the trimer was constructed from the model of the monomer by application of rotation matrices about the noncrystallographic 3-fold axis. Each subunit of the trimer was then refined as a rigid body, to optimize the initial fit, and then positional and B factor refinement was carried out. When the refinement converged, a map was calculated using coefficients $2\,||F_{obs}|-|F_{calc}||\,me^{-i\alpha p}$

TABLE II. Refinement Statistics*

	Resolution (Å)	Number of atoms	Number of residues	R_{TNT} (all data <10 Å)	Combined FOM
Isomorphous model	2.5	9036	438	0.527	0.57†
COMB1	2.5	9036	438	0.291	0.76
COMB2	2.5	9717	446	0.295	0.77
COMB3	2.5	9807	449	0.268	0.78
CON1	1.96	8784	397	0.261	0.74
CON2	1.96	9186	419	0.248	0.75
CON3	1.96	9459	432	0.236	0.75
COMB4	1.96	9798	449	0.227	0.76 (0.81 at 2.5 Å)

*The initial model was built to AVMAP2 at 2.5 Å and was subsequently refined using the TNT protocol; COMB1, COMB2, and COMB3 were intermediate models in the refinement. CON1, CON2, and CON3 were models from which certain atoms had been omitted in the region 260 to 312 in order to determine unambiguously the connectivity. R_{TNT} is the refinement R factor = $\Sigma|(|F_o|-|F_c|)|/\Sigma|F_o|$ and FOM is the overall figure of merit for the combined isomorphous and calculated phases. COMB4 is the model described in this paper.
†No phase combination.

with phases and figures of merit derived from a combination of calculated and isomorphous phase information,[40] without further molecular averaging. The model of a subunit was rebuilt to this map, including the addition of extra side chain atoms where possible, and the whole process repeated for a total of 3 rounds at 2.5 Å.

At this resolution a region of ambiguity in the polypeptide chain trace remained between residues 261 and 311. To resolve this, further cycles of refinement were undertaken using the 1.96 Å data on a partial model from which the above residues had been omitted. Following convergence of the refinement a map was calculated using coefficients as before. In this case, since there was no isomorphous phase information for the data in the 2.5 Å to 1.96 Å shell, a figure of merit was assigned to these reflections following the weighting scheme of Sim.[41] The model was gradually assembled in this region by inclusion of additional stretches of residues only when their appearance in the map gave rise to an unambiguous interpretation of the chain. For example, the directions of the α-helices were determined from the appearance of the carbonyl bulges in the map associated with the main chain peptide groups and the characteristic direction of the side chains which tend to point to the N-terminal end of the helix. In all a total of 3 rounds of refinement and rebuilding were necessary to complete the model (Table II). This procedure resulted in a modification of the chain trace to this part of the polypeptide chain compared to the tentative interpretation based on the 3.7 Å data.[42]

The completed model was then subjected to a further round of refinement at 1.96 Å resolution and a representative portion of the final electron density map is shown in Figure 1. At this stage of the refinement the side chains of some 27 sequenced residues, largely found on the surface of the enzyme, have not been defined completely in the electron density map and we have chosen not to incorporate these into the model. The only other differences affect residues P63, F199, D313, and V426 which are interpreted as proline, phenylalanine, aspartate, and valine, respectively, on the basis of the electron density map rather than the valine, glutamine, alanine, and alanine shown in the chemical sequence.

Details which serve to confirm the interpretation of the molecular structure are strong carbonyl bulges for many residues which serve to fix the direction of secondary structure elements, a buried salt bridge between D160 and R78X which is conserved over all the known hexameric GDH sequences, the match of known cysteine residues to the mercury-binding positions, the grouping of hydrophobic residues into the core of the protein, and the clustering in the three-dimensional structure of residues conserved over the sequenced hexameric GDHs.

The R factor for the atomic structure presented below stands at 0.227 for all data in the range 10 to 1.96 Å resolution and refinement statistics are shown in Tables II and III.

RESULTS AND DISCUSSION

GDH Structure

The 449 residues comprising the polypeptide chain of the GDH subunit are organized into two domains separated by a deep cleft (Fig. 2). Domain I consists of the N-terminal portion of the polypeptide chain (residues 1 to 200) and residues 423 to the C-terminus. The second smaller domain, domain II, is assembled from the contiguous stretch of residues from 201 to 366. The two helices α_{15} and α_{16} (residues 367–422) serve to link the domains and, together with the loop between βf and α9, provide the majority of the interactions between the domains. In all, the structure contains 17 helices and 13 β-strands, with 253 and 86 residues in each conformation respectively, which accounts in total for 75% of

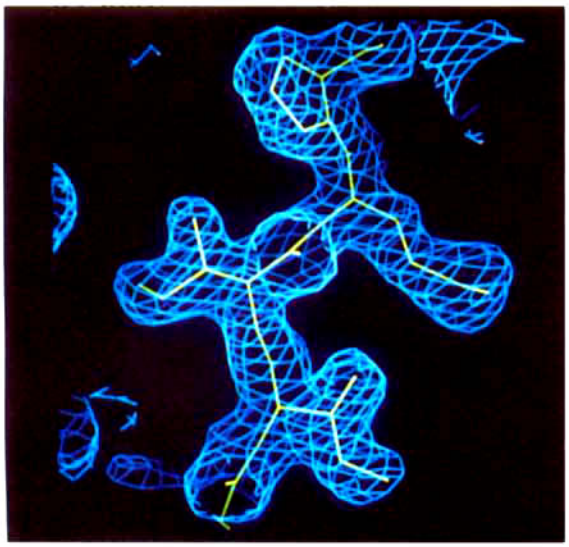

Fig. 1. A portion of the $2||F_{OBS}|-|F_{CALC}||$ electron density map at 1.96 Å, calculated using the COMB4 phase set, viewed edge on to β-strand *k* in domain II. Residues I314, I315, M316, and F317 are shown, bottom to top, in green and the electron density, contoured at an arbitrary level, as blue chicken wire.

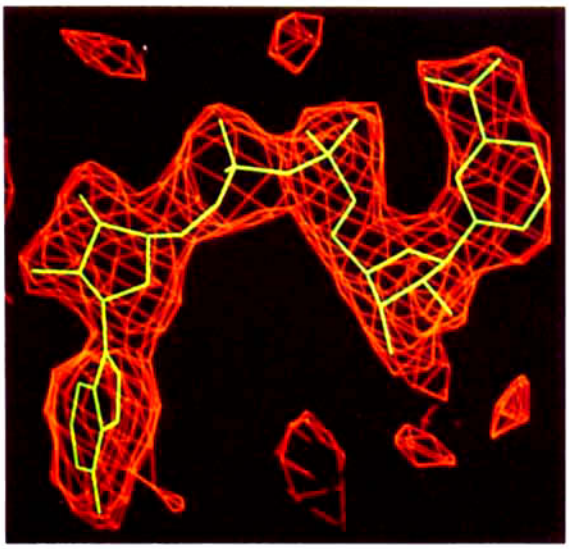

Fig. 6. The positive difference electron density for the binary complex of the enzyme with NAD^+, red, together with the fitted molecular model of NAD^+, green.

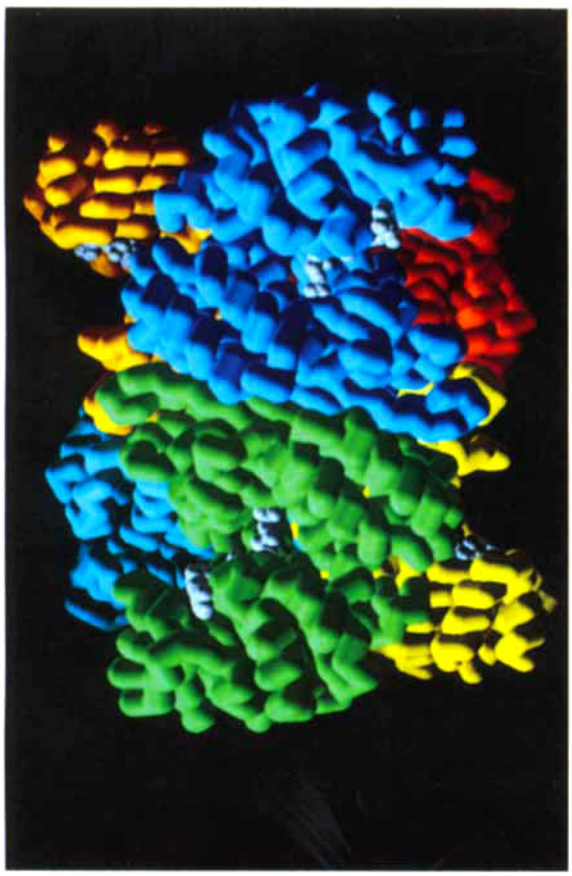

Fig. 5. A schematic space filling model of the GDH hexamer, calculated with the WINSOM modeling package from the α-carbon coordinates, viewed down a crystallographic 2-fold axis. Each subunit is shown in a different color with a van der Waals surface of the bound substrates in white. In the foreground blue subunit the adenine moiety of NAD^+ can be seen edge on; the glutamate lies almost vertical in the center of the subunit.

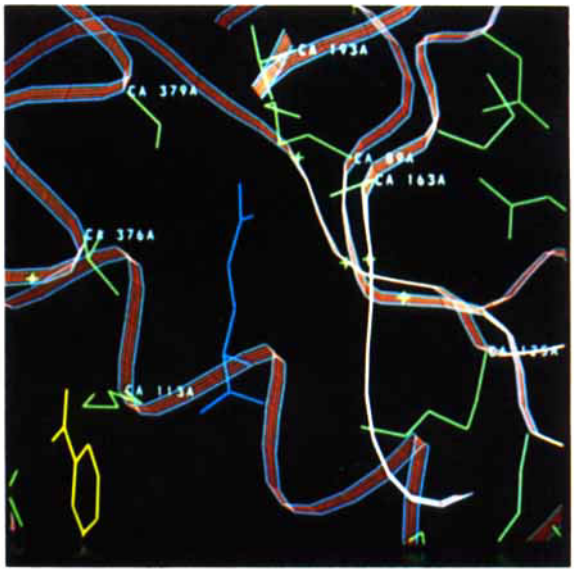

Fig. 7. The proposed active site for GDH. The polypeptide fold is shown as a ribbon, with side chains of residues conserved over all sequenced hexameric GDHs highlighted in green, conserved glycine residues occur as crosses. The bound NAD^+ cofactor is portrayed, yellow, together with the proposed model for the second substrate, glutamate, in blue.

the polypeptide chain. The relationship of the secondary structural elements to their positions in the primary sequence is given in Figure 3. The main chain dihedral angles are given for glycine and nonglycine residues as a Ramachandran plot in Figure 4. Although torsion angles were not restrained in the refinement, the nonglycine residues cluster in the favorable α-helical and β-sheet regions. There are currently four nonglycine residues in the quad-

TABLE III. Deviations From Ideal Geometry of the Model COMB4

Restraint	Unweighted deviation	
	Mean	rms
Bond length (Å)	0.010	0.035
Bond angles (°)	0.595	4.750
Trigonal atom nonplanarity (°)	−0.018	0.024
Planar groups (Å)	−0.024	0.027
Bad contacts (Å)	0.182	0.249

rant of the Ramachandran plot with $\phi > 0$ and $\psi < 0$ which is generally accepted to be nonaccessible. These residues (A306X, S307X, A360X, A361X) all occur in unsequenced loops in the structure where the electron density is poor and the interpretation is necessarily uncertain.

The initial part of domain I is formed by the folding of residues 1 to 51 into a cluster of five helices. A striking feature which follows immediately is the organization of residues 56 to 81 into two antiparallel strands each ~ 35 Å in length, one of which has an exposed edge lying in the molecular surface of the subunit. The polypeptide chain then folds into a series of alternating α/β secondary structural units. The core of this domain is formed by the central β-sheet of 6 strands, which has both parallel and antiparallel elements. The sheet is flanked by helices on both sides. The strand order of this sheet is similar to that of the β-sheet in carboxypeptidase A,[43] however, other details of the molecular structures are not equivalent in three dimensions, with the helices in the two proteins being in different orientations and the lengths of the strands being substantially different.

The chain enters domain II at residue 201. This domain consists of a predominantly parallel central seven-stranded β-sheet which again is flanked by α-helices. The folding pattern of this domain is highly reminiscent of the dinucleotide binding fold, found in many other protein structures,[44,45] though with the direction of one of the strands reversed. Following the final strand in the sheet, the polypeptide chain folds into two helices (α15 and α16) which play an important role in the domain interface. Finally, the chain reenters domain I with the C-terminal helix, α17.

Subunit Assembly

In this oligomeric enzyme six subunits assemble into a hexamer with 32 symmetry (Fig. 5), which can be represented as a squat cylinder of dimensions 108 Å in the direction of the molecular 3-fold axis of symmetry and radius 44 Å across the widest part of the molecule. The two domains of each subunit lie virtually on top of one another in the direction of the 3-fold axis, with domain I closest to the 32 symmetry point and playing the major role in all intersubunit interactions. During the assembly of the hexamer three distinct interfaces have to be considered. These are the dimer interface, the trimer interface, and the additional contact area formed when the hexamer is constructed either from three dimers or two trimers. Since the model does not currently comprise the complete amino acid sequence, calculations of the accessible surface area can only provide a guide to the relative sizes of the different interfaces. Nevertheless, even at this stage, such calculations can be used to indicate the relative importance of the different interfaces. The accessible surface areas were calculated for the monomer, dimer, trimer, and hexamer using the algorithm of Lee and Richards.[46] The total interface per subunit about the 2-fold axis, A_D, was calculated as $(A_{monomer} - A_{dimer}/2) = 1300$ Å^2, which amounts to some 7% of the total surface of the monomer. The interface area per subunit about the threefold axis, A_T, was calculated as $(A_{monomer} - A_{trimer}/3) = 2400$ Å^2, some 13% of the surface area of the monomer. The 32 interface was calculated as the accessible surface area of the hexamer per subunit ($A_H = A_M - A_{hexamer}/6$) less the accessible surface areas of the trimer and dimer, which can be represented as $(A_H - A_D - A_T) = 430$ Å^2, some 2% of the total surface area of the monomer. These results show that the more extensive interface is associated with the trimer and hence the molecule is perhaps best thought of as a dimer of trimers, rather than a trimer of dimers.

When a dimer is constructed a face of mixed hydrophobic and hydrophilic character is buried and this interaction includes the formation of an extensive antiparallel interaction between βa and its 2-fold symmetry related mate. This gives rise to a continuation of the β-sheet in domain I across the 2-fold axis producing a structural unit with 12 strands. Central to the trimer interface is a buried salt bridge between D158 and R389 from a 3-fold related subunit, with both of these residues being conserved in the hexameric GDHs from *E. coli*, *S. typhimurium*, and *N. crassa*. This salt bridge is surrounded by an extensive area of hydrophobic interactions which, in turn, is flanked by a region of hydrophilic contacts. Normal to the direction of the 3-fold axis the surface of the trimer is not planar, but rather the top of each subunit slopes to provide a sawtooth profile producing a surface which is strongly interlocked as the two trimers assemble to form the hexamer (shown schematically in Fig. 2). In the assembled hexamer, an approximately spherical cavity of radius 11 Å is present at the 32 symmetry point. The surface of this cavity, which is lined by hydrophilic residues, is primarily formed by the C-terminal end of α7b and the loop to βc (residues 152–159) and the C-terminal end of α8 and the loop to βf (residues 180–188) in all six subunits.

In this *C. symbiosum* GDH model there are no contacts involving domain II about the 2-fold or 3-

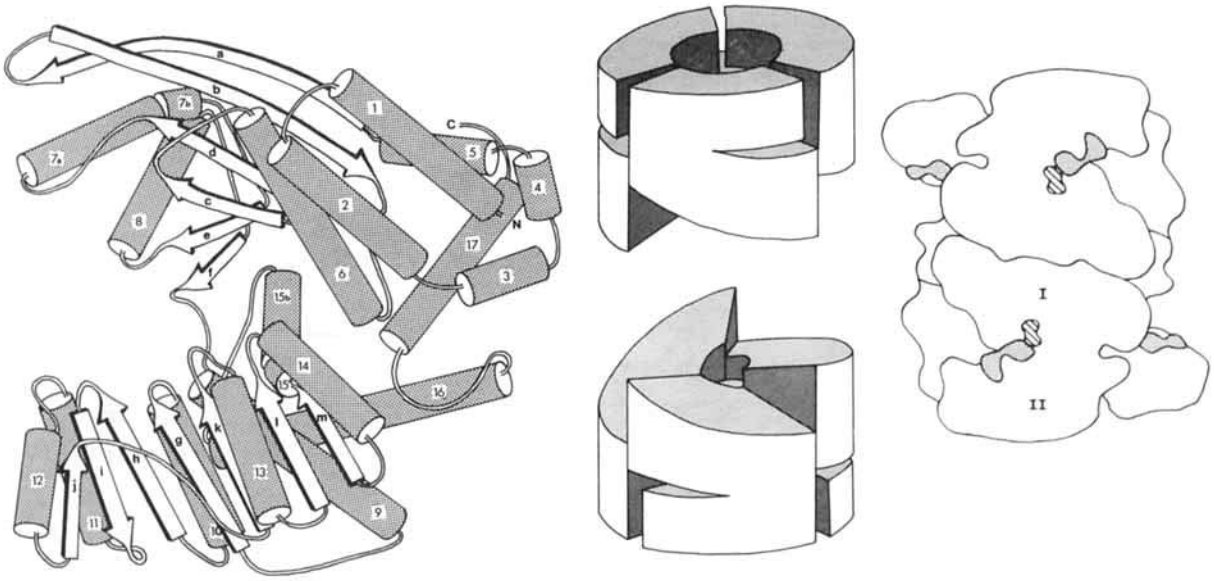

Fig. 2. A schematic representation of the GDH structure; the subunit connectivity is shown, left, with α-helices represented as cylinders and β-sheets as arrows, the positive interlocking of the subunits about the 2-fold axis is illustrated, middle, and the assembly of six subunits into the active hexamer is portrayed, right, with the shaded segments representing the bound cofactor NAD^+ and hatched areas the model of bound glutamate. The two domains of each subunit, I and II, are clearly visible.

fold axes. In the vertebrate GDHs strong sequence homology with other GDHs is lost at the end of α15 and the existence of a secondary structural element equivalent to α16 in the vertebrate enzymes is not certain. However, a plausible alignment of the sequences can be made in which the pattern of hydrophobic and hydrophilic residues is such that a helix is possible at this position. After α16 the sequence homology between the vertebrate and nonvertebrate enzymes is very poor and in addition, the former possess approximately 50 extra residues. The C-terminal end of α16 lies close to the space between the subunits in the region of the dinucleotide binding domain. It is therefore possible that the changes in sequence, coupled with the extra residues, may provide a folding pattern in which additional contacts between the subunits involving domain II are made. If this were to be the case, then a method of communication between the dinucleotide binding domains can be envisaged, which may be the mechanism by which the complex heterotropic allosteric behavior of the vertebrate enzymes is expressed.

Dinucleotide Binding Site

X-Ray analysis on crystals of GDH equilibrated with NAD^+ at 6 Å resolution had previously identified domain II as carrying the determinants for the dinucleotide binding site.[30] A difference Fourier analysis at 2.5 Å on the NAD^+ soaked crystals showed one strong electron density feature per subunit, into which a NAD^+ moiety could be built, together with small scale side chain movements in the vicinity of the dinucleotide. The quality of the map was generally better for one of the three subunits, subunit A. Nevertheless it was sufficiently clear to permit the unambiguous positioning of the adenine ring, the assignment of the adenine ribose conformation to C2′ endo and the clear definition of the two phosphates on the NAD^+ backbone for each of the three subunits. Inspection of the electron density map for subunit A showed the nicotinamide ribose moiety to be in the C2′ endo conformation and the conformation of the nicotinamide ring about the glycosidic bond as *syn*, since the carboxyamide group can be discerned in the map (Fig. 6). For subunits B and C the density in the region of the nicotinamide ring and the associated ribose is not sufficiently good to permit an unambiguous assignment of the conformations, though the fit is consistent with the interpretation given above. It is our belief that the conformational parameters of the NAD^+ and its interaction with the enzyme as determined from subunit A are typical for the *C. symbiosum* GDH and the following discussion is based on the subunit A interpretation. The protein provides a pocket for the adenine ring lined by P262 and T320, with the adenine N3 making a hydrogen bond to the γ-OH of S260, which is conserved in the hexameric GDHs from *E. coli, N. crassa,* and *S. typhimurium*. The 2′- and 3′-hydroxyl groups of the adenine ribose point toward the protein surface with the 2′-OH fitting into a small depression formed by P262 and F238 and hydrogen bonding to the side chain of N289X and the 3′-OH making a hydrogen bond to the main chain NH of F238. OP2 of the nicotinamide phosphate makes a hydrogen bond to the main chain NH

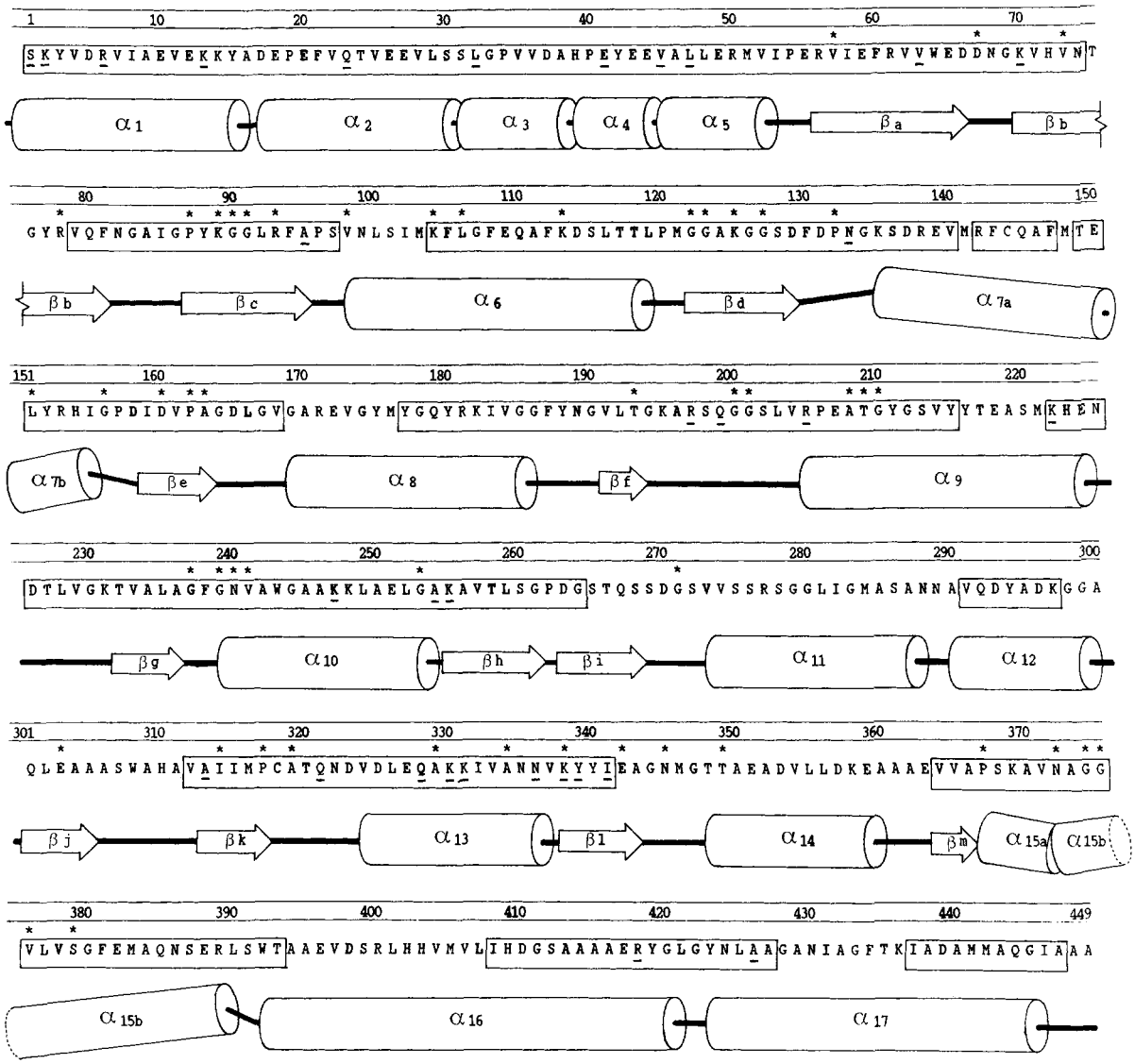

Fig. 3. The relationship of the secondary structure elements (helices as cylinders and strands as arrows) to the primary sequence for the model of *C. symbiosum* GDH. Residues occurring in boxed areas are from sequenced peptides, whereas those without have been deduced from the shape of the electron density coupled to an inspection of the aligned sequences from the hexameric GDHs from bovine liver, rat liver, chicken liver, human liver, *P. asaccharolyticus, E. coli, N. crassa,* and *S. typhimurium;* residues conserved across all these species are starred. Residues in the crystallographic model which have been built differently from the peptide sequence are underlined.

of V241 and the adenine phosphate is stabilized by the helix dipole of α10. With the nicotinamide in the *syn* conformation the NH and the C–O groups of the carboxyamide make hydrogen bonds with δ–O of N240 and γ-OH of T209, respectively, both residues being conserved over all hexameric GDH sequences. In this arrangement, the A face of the nicotinamide ring is packed against the enzyme surface with the A hydrogen at position C4 principally shielded by the γ-methyl of T209. In contrast, the B face of the ring, from which the proton is abstracted during the catalytic cycle,[47,48] is adjacent to a pocket on the enzyme surface containing a striking cluster of conserved residues. There are no steric reasons why the NAD^+ moiety cannot bind with the nicotinamide–ribose bond in the *anti* conformation so as to expose the A face of the ring to this pocket. However, if this were to be the case then there are no residues close enough to the carboxyamide of the ring to provide any stabilizing interactions. Overall, this suggests that a positive selection for the *syn* conformer on the surface of the enzyme is made, rather than a mechanism based on the exclusion of the *anti* conformer by, for example, poor steric contacts.

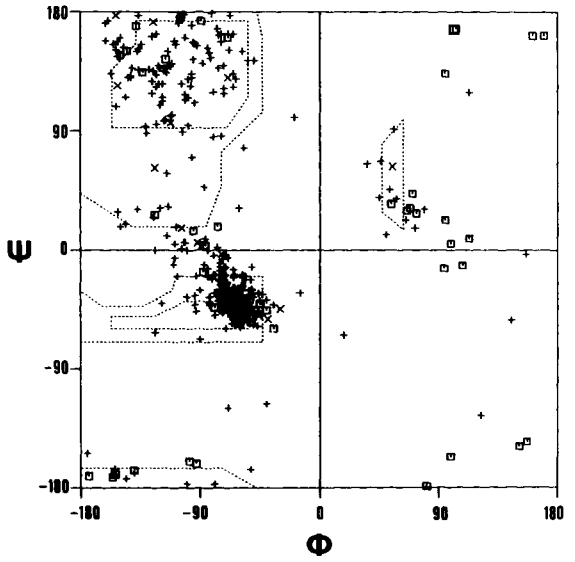

Fig. 4. A Ramachandran plot of the main-chain torsion angles ϕ and ψ. In all 51 glycine residues are shown as squares and 398 other residues as crosses. The four nonglycine residues in the disallowed quadrant with $\phi > 0$ and $\psi < 0$ (A306X, S307X, A360X, A361X) all occur in unsequenced loops in the structure where the electron density is poor and the interpretation is necessarily uncertain.

Structural Relationships to Other Dehydrogenases

The molecular structures of a number of dinucleotide-binding enzymes have been determined and comparisons between their structures and the nature of the interactions with the cofactors have been the subject of a series of investigations. In the particular case of NAD^+-dependent enzymes, the most extensively studied are the class of dehydrogenases which includes lactate dehydrogenase (LDH), s-malate dehydrogenase (s-MDH), glyceraldehyde 3-phosphate dehydrogenase (GPD), and alcohol dehydrogenase (ADH).[45,49] One feature that emerges from the comparison of these enzyme structures is the similar nature of the polypeptide chain organization for the NAD^+-binding domain. The structure of this domain is based on a six-stranded parallel β-sheet (with strand order 321456) flanked by α-helices, in which the connectivity between the β-strands is right handed. This topology is commonly referred to as the Rossmann fold. The conformation of the NAD^+ is very similar in each case except for the glycosidic bond of the nicotinamide ribose which is *anti* for the three A type dehydrogenases, s-MDH, LDH, and ADH and *syn* for the B type dehydrogenase GPD and in all these dehydrogenases the NAD^+ is bound at an equivalent position at the C-terminal end of the β-sheet. The pyrophosphate moiety is located in the crevice formed at the "switch-point" of the β-sheet[50] and is stabilized by a favorable interaction with the so-called "dinucleotide-binding helix."[51,52] When such comparisons are extended to include the dinucleotide-binding domains of enzymes which bind moieties such as FAD^+ or $NADP^+$, different domain topologies are observed. Nevertheless, the common structural feature of all these enzymes is the spatial conservation of a four-stranded parallel β-sheet (strands 1 to 4 of the Rossmann fold) and the "dinucleotide-binding helix" which serves to link the first two β-strands and interacts with the pyrophosphate group.

The model of NAD^+ binding to GDH is generally consistent with these features. The binding site for and the conformation of the NAD^+ are very closely related to that observed in the other dehydrogenases LDH, s-MDH, and ADH and, in particular, given the *syn* conformation of the nicotinamide ribose, to GPD. Furthermore, the pyrophosphate group is stabilized by the dipole of α10, which is the exact spatial equivalent of the "dinucleotide-binding helix" and the hydrogen bonding pattern between the pyrophosphate moiety and this helix is identical to that observed in LDH and GPD. However, in the NAD^+-binding domain of *C. symbiosum* GDH there is one difference in topology, namely the third strand of the sheet (βi) which runs antiparallel with respect to the main sheet direction. Therefore, with respect to the earlier comparisons on the dinucleotide-binding proteins, the secondary structural elements whose relative positions and directions are conserved spatially consist solely of three parallel β-strands and the dinucleotide binding helix. It is interesting to compare this difference in topology with respect to the Rossmann fold with the secondary structure predictions for GDH. Rossmann identified the first two strands of the dinucleotide-binding domain, together with their linking helix, but did not report a satisfactory alignment for the remainder of the domain,[44] which can now be understood by the different connectivity in GDH after the second strand with respect to the other dehydrogenases.

Dinucleotide Specificity

This model for NAD^+ binding permits some conclusions to be drawn on the dinucleotide specificity of members of the GDH family. In particular for this enzyme, the 2′-OH to which the phosphate is attached in $NADP^+$ is placed in a pocket which is too small to allow the phosphate to be accommodated and provides no groups able to stabilize the negative charge. F238 and P262 correspond to serine residues in the $NADP^+$-dependent enzymes of *E. coli, S. typhimurium,* and *N. crassa.* This creates more space near the 2′ position and at the same time provides the potential for stabilizing hydrogen bonds for the phosphate moiety. Furthermore, N289X, which contributes to the NAD^+ specificity in the *C. symbiosum* enzyme, occurs in a region of the sequence (between α11 and α12) which varies consid-

erably in the enzymes from other sources and these differences may have important implications in the determination of coenzyme specificity in the family of GDHs.

Recently, Scrutton and co-workers[53] have redesigned the dinucleotide binding site of *E. coli* glutathione reductase (GTR), constructing a mutant with a pronounced specificity for NAD^+ rather than the natural coenzyme $NADP^+$. Their work, which was based on a sequence analysis of a number of $NADP^+$- and NAD^+-binding enzymes, highlighted the apparent importance in the nucleotide specificity of the sequence pattern in the nucleotide fingerprint region.[52] From their analysis, $NADP^+$-linked enzymes seemed to have the fingerprint pattern GxGxxA, whereas NAD^+-linked enzymes appeared to have a fingerprint sequence GxGxxG together with a carboxyl group towards the C-terminal end of β-strand 2 in the dinucleotide-binding fold to hydrogen bond to the adenine ribose hydroxyl groups. In their mutagenesis of the $NADP^+$-dependent GTR, the substitution A179G (the last residue in the above pattern in this enzyme) had a profound effect on the coenzyme specificity, markedly increasing the affinity for NAD^+. However, this pattern of sequence homology is not found in our NAD^+-linked *C. symbiosum* GDH, with this enzyme having an alanine rather than a glycine in the final position of the fingerprint region. Furthermore, the residue which in other NAD^+-linked dehydrogenases carries the carboxyl group associated with the adenine ribose recognition is replaced by a glycine, and, moreover, in the dual specificity and $NADP^+$-linked GDHs a glutamate or aspartate residue is present at this position. It would therefore appear that the sequence patterns governing the nucleotide specificity are more complex than previously indicated and that there may be various alternative ways of achieving the differential recognition of these important cofactors.

Active Site Model

Data have been collected and processed on crystals soaked in a number of coenzyme and substrate solutions, however, as yet no direct crystallographic evidence on the binding of either glutamate or 2-oxoglutarate has been obtained. This may be due to interference by the high concentration of either sulfate or ammonium ions present in the solution from which the crystals were grown, especially since ammonia is a substrate of the enzyme. Therefore, we have analyzed the pattern of sequence conservation across members of the hexameric GDH family in order to identify residues involved in substrate binding and catalysis. The pattern of conserved residues highlights the importance of the cleft between the two domains where considerable clustering of sequence conservation occurs in the three-dimensional structure. Given the negative charges present on the glutamate/2-oxoglutarate moiety, it might be expected that the enzyme would provide positive charges to stabilize substrate binding and we have looked particularly for conservation of lysine, arginine, and histidine residues. There are only seven such conserved residues in the aligned sequences of the hexameric GDHs, and, moreover, four of these (K89, R93, K113, and K125) are close together in a pocket next to the B face of the nicotinamide ring. We have attempted to model interactions between the glutamate moiety and this cluster of conserved residues. Given that there may be conformational changes in the protein structure on glutamate binding, arrangements with suboptimal distances for interactions such as salt bridges and hydrogen bonds are not necessarily precluded and therefore many possible orientations for the substrate can be envisaged. Nevertheless, one model for glutamate binding seems particularly plausible, which is shown in Figure 7. This involves a conformation for the glutamate moiety which is fully extended and therefore maximises the separation between the C1 and C5 carboxyl groups. In this model the C1 carboxyl is 3 to 3.5 Å from the NH_3^+ groups of K113 and K125, while the C5 carboxyl is a similar distance from the NH_3^+ of K89, the γ-OH of S379 and the γ-OH of T193. The 2 amino group of the glutamate is ~4.0 Å from the main chain carbonyl of G164 and, together, the side chains of V376 and A163 form hydrophobic interactions with the C3, C4, and C5 carbons of the glutamate. In the sequenced hexameric GDHs, all these residues are conserved, with the exception of G164, which can be either glycine or proline. The conformation of the glutamate moiety in this model is closely resembled by isophthalate, a potent inhibitor of bovine GDH,[54] which binds ~1,000 times tighter than glutamate, and has its carboxyl groups locked in an extended conformation by the aromatic ring. This model also provides a role for K125, which has been implicated for so long in the activity of this enzyme.[3,13,28,55,56] Moreover, the cluster of three conserved lysines, 89,113, and 125 corresponds precisely with the group of three essential residues identified independently by modification with pyridoxal 5′-phosphate.[57] However, the uncertainty associated with the mode of glutamate binding currently provides a severe restriction on the assignment of the functional roles of the conserved residues in terms of substrate binding and catalysis. This model places the Cα of the glutamate 6.3 Å from the C_4 of the nicotinamide ring, from which the proton is abstracted during the catalytic cycle. Clearly, a small conformational change is required to position the nicotinamide ring sufficiently close to the substrate for catalysis, but, given that the two domains are not linked by any complex arrangement of secondary structural elements, domain movements upon substrate binding remain a distinct possibility. Finally, we note that despite the

similarity in the topology of the β-sheet in domain I of GDH, which provides many of the residues involved in glutamate binding, with the β-sheet in carboxypeptidase A, the active sites of these two enzymes are on topologically opposite sides of the sheet and hence the resemblance does not extend to one of functional significance.

The determination of the structure of GDH has provided a framework around which the extensive biochemical and biophysical data accumulated on this enzyme can begin to be correlated, and, to test our active site model, a new crystal form, obtained by salting out the protein using sodium glutamate as the precipitant, is now under investigation.

ACKNOWLEDGMENTS

We thank Paul Brown and Fiona Rodgers for technical assistance, the support staff at the Synchrotron Radiation Source at Daresbury for help with station alignment, and Geoffrey Ford for help with the WINSOM modeling package, kindly loaned by Peter Quarendon of IBM Winchester. This work was supported by grants from the Science and Engineering Research Council and Medical Research Council of the United Kingdom. D.W.R. is a Lister Institute Research Fellow. K.S.L. was supported by a University of Sheffield Postgraduate Scholarship. The Krebs Institute is an S.E.R.C. designated center for molecular recognition.

REFERENCES

1. Frieden, C. Glutamate dehydrogenases. In: "The Enzymes," 2nd ed., Vol. 7. Boyer, P.D. (ed.). New York: Academic Press, 1963: 3–24.
2. Braunstein, A.E. Les voies principales de l'assimilation et dissimilation de l'azote chez les animaux. Adv. Enzymol. 19:335–389, 1957.
3. Smith, E.L., Austen, B.M., Blumenthal, K.M., and Nyc, J.F. Glutamate Dehydrogenases. In: "The Enzymes," 3rd ed. Vol 11. Boyer, P.D. (ed.). New York: Academic Press, 1975: 293–367.
4. Uno, I., Matsumoto, K., Adachi, K., Ishikawa, T. Regulation of NAD-dependent glutamate dehydrogenase by protein kinases in *Saccharomyces cerevisiae*. J. Biol. Chem. 259:1288–1293, 1984.
5. Veronese, F.M., Nyc, J.F., Degani, Y., Brown, D.M., Smith, E.L. Nicotinamide adenine dinucleotide-specific glutamate dehydrogenase of *Neurospora*. J. Biol. Chem. 249(24):7922–7928, 1974.
6. Hornby, D.P., Engel, P.C. Characterization of *Peptostreptococcus asaccharolyticus* glutamate dehydrogenase purified by dye-ligand chromatography. J. Gen Microbiol. 130: 2385–2394, 1984.
7. Rice, D.W., Hornby, D.P., Engel, P.C. Crystallization of an NAD^+-dependent glutamate dehydrogenase from *Clostridium symbiosum*. J. Mol. Biol. 181:147–149, 1985.
8. McPherson, M.J., Wootton, J.C. Complete nucleotide sequence of the *Escherichia coli gdhA* gene. Nucl. Acids. Res. 11:5257–5266, 1983.
9. Wootton, J.C., Chambers, G.K., Holder, A.A., Baron, A.J., Taylor, J.G., Fincham, J.R.S., Blumenthal, K.M., Moon K., Smith, E.L. Amino-acid sequence of NADP-specific glutamate dehydrogenase of *Neurospora crassa*. Proc. Natl. Acad. Sci. U.S.A. 71(11):4361–4365, 1974.
10. Bansal, A., Dayton, M.A., Zalkin, H., Colman, R.F. Affinity labelling of a glutamyl peptide in the coenzyme binding site of $NADP^+$-specific glutamate dehydrogenase of *Salmonella typhimurium* by 2-[(4-bromo-2,3-dioxobutyl)thio]-1,N^6-ethenoadenosine 2′,5′-bisphosphate. J. Biol. Chem. 264(17):9827–9835, 1989.
11. Moon, K., Piszkiewicz, D., Smith, E.L. Glutamate dehydrogenase amino-acid sequence of the bovine enzyme and comparison with that from chicken liver. Proc. Natl. Acad. Sci. U.S.A. 69:1380–1383, 1972.
12. Julliard, J.H., Smith, E.L. Partial amino acid sequence of the glutamate dehydrogenase of human liver and a revision of the sequence of the bovine enzyme. J. Biol. Chem. 254:3427–3438, 1979.
13. Wootton, J.C. The coenzyme-binding domains of glutamate dehydrogenases. Nature (London) 252:542–546, 1974.
14. Piszkiewicz, D., Landon, M., Smith, E.L. Bovine glutamate dehydrogenase. Loss of allosteric inhibition by guanosine triphosphate and nitration of tyrosine-412. J. Biol. Chem. 246:1324–1329, 1971.
15. Coffee, C.J., Bradshaw, R.A., Goldin, B.R., Frieden, C. Identification of the sites of modification of bovine liver glutamate dehydrogenase reacted with trinitrobenzenesulphonate. Biochemistry 10:3516–3526, 1971.
16. Goldin, B.R., Frieden, C. Effect of trinitrophenylation of specific lysyl residues on the catalytic, regulatory and molecular properties of bovine liver glutamate dehydrogenase. Biochemistry 10:3527–3534, 1971.
17. Smith, E.L. Evolution of the structure and function of glutamate dehydrogenases. In: "Multidomain Proteins." Pathy, L., Friedrich, P. (eds.). Budapest: Akademiai Kiado, 1986: 35–48.
18. Birktoft, J.J., Miake.F, Frieden, C., Banaszak, L.J. Crystallographic studies of glutamate dehydrogenase. J. Mol. Biol. 138:145–148, 1980.
19. Veronese, F.M., Boccu, E., Conventi, L. Glutamate dehydrogenase from *Escherichia coli:* Induction, purification and properties of the enzyme. Biochim. Biophys. Acta 377: 217–228, 1975.
20. Ifflaender, U., Sund, H. Association behaviour of rat liver glutamate dehydrogenase. FEBS Lett. 20:287–290, 1972.
21. Ashby, B., Wootton, J.C., Fincham, J.R.S. Slow conformational changes of a *Neurospora* glutamate dehydrogenase studied by protein fluorescence. Biochem. J. 143:317–329, 1974.
22. Neumann, P., Markau, K., Sund, H. Studies of glutamate dehydrogenase regulation of glutamate dehydrogenase from *Candida utilis* by a pH and temperature-dependent conformational transition. Eur. J. Biochem. 65:465–472, 1976.
23. Syed, S.-E.-H., Engel, P.C. Reversible pH-dependent inactivation of glutamate dehydrogenase from *Clostridium symbiosum*. Biochem. Soc. Trans. 14:157, 1986.
24. Goldin, B.R., Frieden, C. L-Glutamate dehydrogenases. Curr. Top. Cell Reg. 4:77–117, 1971.
25. Fisher, H.F. Glutamate dehydrogenase-ligand complexes and their relationship to the mechanism of the reaction. Adv. Enzymol. 39:369–417, 1973.
26. Sund, H., Markau, K., Koberstein, R. Glutamate dehydrogenase. In: "Subunits in Biological Systems," Vol. 7. Timasheff, S., Fasman, G.D. (eds.). New York: Marcel Dekker, 1975: 226–287.
27. Bayley, P.M., O'Neill, K.T.J. The binding of oxidised coenzyme to bovine-liver glutamate dehydrogenase studied by circular-difference spectroscopy. Eur. J. Biochem. 112: 521–531, 1980.
28. Gore, M.G. L-Glutamic dehydrogenase. Int. J. Biochem 13: 879–886, 1981.
29. McPherson, M.J., Baron, A.J., Jones, K.M., Price, G.J., Wootton, J.C. Multiple interactions of lysine-128 of *Escherichia coli* glutamate dehydrogenase revealed by site-directed mutagenesis studies. Protein Eng. 2:147–152, 1988.
30. Rice, D.W., Baker, P.J., Farrants, G.W., Hornby, D.P. The crystal structure of glutamate dehydrogenase from *Clostridium symbiosum* at 0.6nm resolution. Biochem. J. 242:789–795, 1987.
31. North, A.C.T., Phillips, D.C., Matthews, F.S. A semi-empirical method of absorption correction. Acta Crystallogr. A24:351–359, 1968.
32. Fox, G.C., Holmes, K.C. An alternative method of solving the layer scaling equations of Hamilton, Rollett and Sparks. Acta Crystallogr. 20:886–891, 1966.
33. Baker, P.J., Farrants, G.W., Stillman, T.J., Britton, K.L., Helliwell, J.R., Rice, D.W. Isomorphous replacement with

optimized anomalous scattering applied to protein crystallography. Acta Crystallogr. A46:721–725, 1990.
34. CCP4, The S.E.R.C. (U.K.) Collaborative Computing Project no. 4. A Suite of Programs for Protein Crystallography, distributed from Daresbury Laboratory, Warrington, WA4 4AD, U.K., 1979.
35. Dodson, E., Vijayan, M. The determination and refinement of heavy-atom derivatives. Some model calculations using acentric reflexions. Acta Crystallogr. B27: 2402–2411, 1971.
36. Bricogne, G. Methods and programs for direct-space exploitation of geometric redundancies. Acta Crystallogr. A32:832–847, 1976.
37. Dickerson, R.E., Weinzierl, J.E., Palmer, R.A. A least-squares refinement method for isomorphous relplacement. Acta Crystallogr. B24:997–1003, 1967.
38. Jones, A.T. A graphics model building and refinement system for macromolecules. J. Appl. Crystallogr. 11:268–272, 1978.
39. Tronrud, D.E., Ten Eyck, L.F., Matthews, B.W. An efficient general-purpose least-squares refinement program for macromolecular structures. Acta Crystallogr. A43: 489–501, 1987.
40. Rice, D.W. The use of phase combination in the refinement of phosphoglycerate kinase at 2.5 Å resolution. Acta Crystallogr. A37:491–500, 1981.
41. Sim, G.A. The distribution of phase angles for structures containing heavy atoms. II. A modification of the normal heavy-atom method for non-centrosymmetrical structures. Acta Crystallogr. 12:813–815, 1959.
42. Baker, P.J., Farrants, G.W., Rice, D.W., Stillman, T.J. Recent progress on the structure and function of glutamate dehydrogenase. Biochem. Soc. Trans. 15:748–751, 1987.
43. Rees, D.C., Lewis, M., Lipscomb, W.N. Refined crystal structure of carboxypeptidase A at 1.54Å resolution. J. Mol. Biol. 168:367–387, 1983.
44. Rossmann, M.G., Moras, D., Olsen, K.W. Chemical and biological evolution of a nucleotide-binding protein. Nature (London) 250:194–199, 1974.
45. Rossmann, M.G., Liljas, A., Brändén, C-I., Banaszak, L.J. Evolutionary and structural relationships among dehydrogenases. In: "The Enzymes," 3rd ed. Vol. 11. (Boyer, P.D.) (ed.). New York: Academic Press, 1975: 61–102.
46. Lee, B., Richards, F.M. The interpretation of protein structures: Estimation of static accessibility. J. Mol. Biol. 55: 379–400, 1971.
47. You, K-S. Stereospecificity for nicotinamide nucleotides in enzymatic and chemical hydride transfer reactions. CRC Crit. Rev. Biochem. 17(4):313–451, 1985.
48. Srivastava, D.K., Bernhard, S.A., Langridge, R., McClarin, J.A. Molecular basis for the transfer of nicotinamide adenine dinucleotide among dehydrogenases. Biochemistry 24:629–635, 1985.
49. Birktoft, J.J., Banaszak, L.J. Structure-function relationships among nicotinamide-adenine dinucleotide dependent oxidoreductases. In: "Peptide and Protein Reviews," Vol. 4. Hearn, M.T.W. (ed.). New York: Dekker, 1984: 1–46.
50. Brändén, C-I. Relation between structure and function of α/β proteins. Q. Rev. Biophys. 13(3):317–338, 1980.
51. Hol, W.G.J., van Duijen, P.T., Berendsen, H.J.C. The α-helix dipole and the properties of proteins. Nature (London) 273:443–446, 1978.
52. Wierenga, R.K., De Maeyer, M.C.H., Hol, W.G.L. Interaction of pyrophosphate moieties with α-helices in dinucleotide binding proteins. Biochemistry 24:1346–1357, 1985.
53. Scrutton, N.S., Berry, A., Perham, R. Redesign of the coenzyme specificity of a dehydrogenase by protein engineering. Nature (London) 343:38–43, 1990.
54. Caughey, W.S., Smiley, J.D., Hellerman, L. L-Glutamic acid dehydrogenase structural requirements for substrate competition: Effect of thyroxine. J. Biol. Chem. 224:591–607, 1957.
55. Rife, J.E., Cleland, W.W. Kinetic mechanism of glutamate dehydrogenase. Biochemistry. 19:2321–2333, 1980.
56. Chen, S-S., Engel, P.C. The equilibrium position of the reaction of bovine liver glutamate dehydrogenase with pyridoxal 5′-phosphate. Biochem. J. 147:351–358, 1975.
57. Lilley, K.S., Engel, P.C. Identification of lysine residues involved in substrate binding at the active site of the NAD^+-dependent glutamate dehydrogenase of *Clostridium symbiosum*. Biochem. Soc. Trans. 16:875–876, 1988.
58. Lilley, K.S., Baker, P.J., Britton, K.L., Stillman, T.J., Brown, P.E., Moir, A.J.G., Engel, P.C., Rice, D.W., Bell, J.E., Bell, E. The partial amino acid sequence of the WAD^+-dependent glutamate dehydrogenase of *Clostridium symbosium*. Implications for the evolution and structural basis of coenzyme specificity. Biochim. Biophys. Acta 1080:191–197, 1991.